

Non-Fermi liquid behaviour in non-equilibrium transport through Co doped Au chains connected to four-fold symmetric leads

S. Di Napoli,¹ P. Roura-Bas,¹ Andreas Weichselbaum,² and A. A. Aligia³

¹*Dpto de Física, Centro Atómico Constituyentes,
Comisión Nacional de Energía Atómica, Buenos Aires, Argentina*

²*Ludwig-Maximilians-Universität München, 80333 Munich, Germany*

³*Centro Atómico Bariloche and Instituto Balseiro,
Comisión Nacional de Energía Atómica, 8400 Bariloche, Argentina*

We calculate the differential conductance as a function of temperature and bias voltage, $G(T, V)$, through Au monoatomic chains with a substitutional Co atom as a magnetic impurity, connected to a four-fold symmetric lead. The system was recently proposed as a possible scenario for observation of the overscreened Kondo physics. Stretching the chain, the system could be tuned through a quantum critical point (QCP) with three different regimes, overscreened, underscreened and non Kondo phases. We present calculations of the impurity spectral function by using the numerical renormalization group (NRG) for the three different regimes characterizing the QCP. Non trivial behaviour of the spectral function is reported near the QCP. Comparison with results using the non crossing approximation (NCA), shows that the latter is reliable in the overscreened regime, when the anisotropy is larger than the Kondo temperature. For these parameters, which correspond to realistic previous estimates, $G(T, V)$ calculated within NCA exhibits clear signatures of the non-Fermi liquid behaviour within the overscreened regime.

PACS numbers: 73.23.-b, 71.10.Hf, 75.20.Hr

I. INTRODUCTION

The Fermi liquid (FL), or the Landau-Fermi liquid theory, is on the basis of our understanding of many properties of the metal state at sufficient low temperatures. For instance, the electrons in a normal, non-superconducting, metal at low temperatures behave as a FL. Also, magnetic impurities with spin $S_I = 1/2$ embedded in a non-magnetic metal exhibit the Kondo anomaly, that could be theoretically explained by the one-channel Kondo (1CK)¹ and one-channel Anderson (1CA)² models. Both models lead to a ground state that can be described by a FL. Even for low dimensional systems, such as quantum dots coupled to metallic leads, transport measurements at low temperatures were found in agreement with FL predictions. Specifically, conductance through a single-electron transistor at low temperature is in quantitative agreement with the calculated one from the Anderson impurity model³.

On the contrary, the non-Fermi liquid (NFL) paradigm describes a system which displays a breakdown of the Fermi-liquid properties. A large class of heavy fermions materials, such as Ce and U alloys are examples of a metallic state that is not a Fermi-liquid^{4,5}. Exotic properties of these alloys at low temperature, such as significant residual entropy and non-saturated magnetic susceptibility can be understood on the basis of the two-channel Kondo (2CK) model introduced early by Nozières and Blandin⁶, which is one example of the NFL quantum impurity model. In low dimensions, the simplest example of NFL is the Luttinger liquid, given by interacting fermions in one dimension⁷.

From the experimental point of view, the realization of the two-channel (2C) state was studied in a double

dot system proposed by Oreg and Goldhaber-Gordon,^{8,9} who showed that the differential conductance as a function of bias voltage V follows a \sqrt{V} behaviour, which is, again, characteristic of 2C physics⁹. Much theoretical work have been done,^{10,11}, in order to develop a theory of such experimental setup on the basis of the two channel Anderson (2CA) Hamiltonian. In this model, two symmetric independent electron modes screen a localized level with spin $S_I = 1/2$. Among other interesting properties coming up from this model, both, the impurity contribution to the entropy at zero temperature, $S = \frac{1}{2} \ln(2)$, and the conductance per channel at low-temperatures, $G(T) \simeq a - b\sqrt{T}$, display a NFL behaviour,¹²⁻¹⁴. The key property to observe the NFL signatures in the above mentioned experiment was the setup capability to control the coupling constants between the dot and two independent reservoirs, J_1, J_2 , to make them symmetric ones, $J_1 \sim J_2$. The requirement of symmetry between the scattering channels,⁶, is very difficult to achieve in real materials, making the NFL observation hard to find.

Recently, two different realizations of a 2CK effect, with a robust symmetry between the two conduction channels have been proposed^{15,16}. In Ref. 15, Tsvelik *et al.* show a possible realization of the overscreened multi-channel Kondo model in a system of spin chains. In this model, N spin $S = 1/2$ Heisenberg chains interact with a cluster of N extra spins $1/2$. Some interesting examples of real materials that could exhibit the necessary symmetry between the scattering channels were proposed¹⁵. In Ref. 16 a four-fold symmetric Co doped Au chain was proposed as a scenario to exhibit NFL behaviour by Di Napoli *et al.*. The Co atom, considered as a magnetic impurity, mix the $3d^7$ and $3d^8$ configurations through the hopping with $5d_{xz}$ and $5d_{yz}$ electrons

of Au, that play the role of two independent and symmetric scattering channels. The broken axial symmetry along the chain by a four-fold symmetric crystal field is an essential ingredient to observe the NFL signatures. Stretching the system might be a way to pass through a quantum critical point (QCP) that divide three different phases, overscreened, underscreened and finally another one without Kondo effect. Specifically, within the overscreened regime, two different properties of the NFL behaviour have been found: the conductance per channel as a function of temperature through the Co following a $G(T) \simeq a - b\sqrt{T}$ form and the Co entropy contribution having a residual value of $S = \frac{1}{2} \ln(2)$ at zero temperature.

The purpose of the present contribution is to complement the study of the Co-Au chain model with properties not shown in Ref. 16. First, we present calculations of the impurity spectral function obtained with the numerical renormalization group (NRG)¹⁷ for the three different phases reinforcing the presence of a QCP. Non trivial behaviour of the spectral density is discussed near to the QCP. Second, we present calculations of the differential conductance, $G(T, V)$, through the Co atom within a non-equilibrium situation by using the non crossing approximation (NCA) solution of the model in its overscreened regime. We obtain that $G(T, V)$ also displays clear signatures of NFL behaviour in this regime. We also show the limitations of the NCA to describe the other regimes and to capture very small energy scales.

The paper is organized as follows. In section II we introduce the model. The different regimes of the system are also discussed. In section III the numerical solution of the model is presented within the NRG and NCA approaches. Finally, in section IV some conclusions are drawn.

II. MODEL

According to *ab-initio* calculations, the Co atom embedded in a Au chain, Fig. 1a, is in a $3d^7$ configuration with the three holes coupled to a total spin $S = 3/2$ ¹⁶. This atomic configuration seems to be robust even if the noble metal changes from Au to Ag and Cu¹⁸. One d -hole is shared between the half filled $3d_{xy}$ and $3d_{x^2-y^2}$ (Δ_4 -symmetry) orbitals while the other two are in the degenerate $3d_{xz}$, $3d_{yz}$ (Δ_3 -symmetry) ones.

According to transport measurements, the pure Au chain only has 6s bands crossing the Fermi level¹⁹. However, the presence of environmental O impurities can push up and stabilize the $5d_{xz}$ and $5d_{yz}$ bands of Au at and above the Fermi level¹⁸. While the Δ_3 symmetries of Au chain can be tuned in order to make these band conductors, there is no similar mechanism to get electrons of Au with Δ_4 symmetry at the Fermi level due to their high localization. Details of the first principle calculations can be found in Refs.^{16,18}.

According to this, the $5d_{xz}$ and $5d_{yz}$ bands of Au repre-

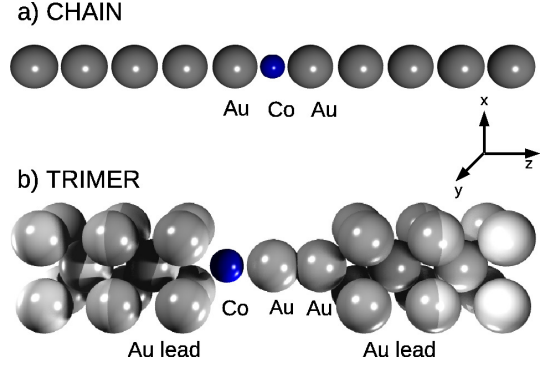


FIG. 1: Sketch of the pure chain with a substitutional Co (a) and a trimer connected to a four-fold symmetric axis leads (b).

sent two independent and symmetric channels that screen the localized moment at the corresponding symmetries of the Co impurity. The Δ_4 -symmetry levels in Co have frozen its charge and spin fluctuations due to the absence of hybridization with the Au neighbours.

As it was previously mentioned in the introduction, in a system with a four-fold symmetric axis such as a trimer with one Co atom connected to body-centered-cubic leads, Fig. 1b, the degeneracy between the $3d_{xy}$ and $3d_{x^2-y^2}$ orbitals of Co is broken localizing the hole in the $3d_{xy}$ orbital. Note that exactly the same physics is obtained if both Δ_4 orbitals are interchanged. The energies of the localized three holes in the Co atom are $E_{xy} = -0.2$ eV and $E_{xz} = E_{yz} = -0.3$ eV, where we set the Fermi level as the zero of energy. The spin-orbit coupling (SOC) in the Co atom induces a splitting D between the projections $S_z = \pm 3/2$ and $S_z = \pm 1/2$ of the quadruplet that belongs to the total spin $S = 3/2$. The calculation of D was exactly done by solving a 120×120 matrix of the Hamiltonian of the $3d^7$ configurations²⁰. For the real parameters of the setup shown in Fig. 1b the value of the anisotropy was found to be $D = 1.7$ meV. While the *ab-initio* calculations¹⁶ have been done in the system represented in Fig. 1b, we want to emphasize that the same physics is expected for any length of the Au chain between the leads.

With this information the effective Hamiltonian that describes the system is given by

$$\begin{aligned}
 H_{\text{eff}} = & (E_3 + \frac{D}{2} M_3^2) \sum_{M_3} |M_3\rangle \langle M_3| + E_2 \sum_{\alpha M_2} |\alpha M_2\rangle \langle \alpha M_2| \\
 & + \sum_{\nu k \alpha \sigma} \epsilon_{\nu k} c_{\nu k \alpha \sigma}^\dagger c_{\nu k \alpha \sigma} + \\
 & \sum_{\alpha \nu k \sigma} V_\nu \langle \frac{3}{2} M_3 | \frac{1}{2}; M_2 \sigma \rangle (|M_3\rangle \langle \alpha M_2| c_{\nu k \alpha \sigma} + \text{H.c.}),
 \end{aligned} \tag{1}$$

where E_n , M_n represent the energies and the spin projections along the chain, which was chosen as the quantization axis, of states with $n = 2, 3$ holes in the $3d$ shell of Co. The term $\langle SM | S_2 S_1; M_2 M_1 \rangle$ stands for the

standard SU(2) Clebsch-Gordan coefficients. The state with three holes and maximum spin projection is denoted by $|3/2\rangle = \hat{d}_{xz\downarrow}^\dagger \hat{d}_{yz\downarrow}^\dagger \hat{d}_{xy\downarrow}^\dagger |0\rangle$, where $|0\rangle$ represents the $3d^{10}$ configuration and the operators $\hat{d}_{\beta\sigma}^\dagger$ create a hole with symmetry β and spin projection σ . The states with two holes in Co can be constructed by removing an α ($\alpha = xz, yz$) hole. For instance, the maximum spin projection of the state with two holes is given by $|\bar{\alpha}, 1\rangle = \hat{d}_{\alpha\downarrow}^\dagger |3/2\rangle$. Then the state $|\bar{\alpha}, 1\rangle$ does not contain the hole with symmetry α , which jumped to the Au band. In other words, if the electron $5d_{xz}$ of Au jumps to the Co, the remaining state $|xy, 1\rangle$ has holes in $3d_{yz}$ and $3d_{xy}$, but not in $3d_{xz}$. The other relevant states with two and three holes can be obtained by using the spin lowering operator.

There are also states with three holes in the Co atom coupled to a total spin $S = 1/2$ in which one of the β -orbitals is doubly occupied but, in view of the obtained *ab-initio* calculations, these can be considered as high excited states.

The operator $c_{\nu k\alpha\sigma}^\dagger$ creates a hole in the $5d$ shell of Au with symmetry α where $\nu = L, R$ denotes the left or the right side of Co atom, respectively. The hopping V_ν defines the hybridization $\Gamma_\nu = 2\pi \sum_k |V_\nu|^2 \delta(\omega - \epsilon_{\nu k})$, neglecting the weak dependence with the energy ω .

Consequently, the Hamiltonian in Eq. 1 describes fluctuations between the quadruplet of the $3d^7$ configuration and two triplets corresponding to the $3d^8$ configuration, with one xy -hole and the other in either $\alpha = yz$ or $\alpha = xz$ symmetries, via the hybridization with the states of symmetry Δ_3 of the Au leads.

The last term in Eq. 1 represents the mixing Hamiltonian, H_{mix} , between the impurity and conducting Au atoms. Writing explicitly the non vanishing Clebsch-Gordan coefficients this becomes,

$$\begin{aligned} H_{mix} = & \sum_{\alpha\nu k\sigma} V_\nu (|\frac{3}{2}\rangle \langle \bar{\alpha}, 1| + \sqrt{\frac{2}{3}} |\frac{1}{2}\rangle \langle \bar{\alpha}, 0| + \\ & \sqrt{\frac{1}{3}} |-\frac{1}{2}\rangle \langle \bar{\alpha}, -1|) c_{\nu k\alpha\uparrow} \\ & + (|-\frac{3}{2}\rangle \langle \bar{\alpha}, -1| + \sqrt{\frac{2}{3}} |-\frac{1}{2}\rangle \langle \bar{\alpha}, 0| + \\ & \sqrt{\frac{1}{3}} |\frac{1}{2}\rangle \langle \bar{\alpha}, 1|) c_{\nu k\alpha\downarrow} + \text{H.c.} \end{aligned} \quad (2)$$

The operator that creates a hole in the $3d$ shell of the Co atom with symmetry α and spin σ can be represented by Hubbard operators between states containing two and three holes. In that case, the two holes forming the triplet are in the xy and $\bar{\alpha}$ orbitals. It can be written as follows

$$\begin{aligned} d_{\alpha\uparrow}^\dagger &= |\frac{3}{2}\rangle \langle \bar{\alpha}, 1| + \sqrt{\frac{2}{3}} |\frac{1}{2}\rangle \langle \bar{\alpha}, 0| + \sqrt{\frac{1}{3}} |-\frac{1}{2}\rangle \langle \bar{\alpha}, -1|, \quad (3) \\ d_{\alpha\downarrow}^\dagger &= |-\frac{3}{2}\rangle \langle \bar{\alpha}, -1| + \sqrt{\frac{2}{3}} |-\frac{1}{2}\rangle \langle \bar{\alpha}, 0| + \sqrt{\frac{1}{3}} |\frac{1}{2}\rangle \langle \bar{\alpha}, 1|. \end{aligned}$$

Then, the hybridization term of the Hamiltonian takes the usual Anderson impurity form, that is

$$H_{mix} = \sum_{\alpha\nu k\sigma} V_\nu (d_{\alpha\sigma}^\dagger c_{\nu k\alpha\sigma} + c_{\nu k\alpha\sigma}^\dagger d_{\alpha\sigma}). \quad (4)$$

Depending on the value of the anisotropy D , interesting and different physics emerges from this Hamiltonian. The role played by D is to split the quadruplet states into two doublets with spin projection $M_3 = \pm 3/2$ and those with $\pm 1/2$. For the case in which the anisotropy vanishes, $D = 0$, in addition to the SU(2) channel symmetry the Hamiltonian also has the rotational spin SU(2) one. For this isotropic case, the model in Eq. 1 reduces to the underscreened impurity Anderson model, in which the two channels with spin $1/2$ compensate a part of the total impurity spin $3/2$. For one channel, the model was solved exactly by Aligia *et al.*, by using the Bethe ansatz²¹ for the spin 1 underscreened one-channel Kondo model, a singular FL ground state was found²². It is natural to expect similar physics our case for $D = 0$, which corresponds to a spin $3/2$ underscreened by two conduction channels. The behavior of the conductance at low temperatures indicates this is actually the case¹⁶.

When the anisotropy takes positive values, as it was found for the realistic case of the setup in Fig. 1b, $D = 1.7$ meV, the doublet with $M_3 = \pm 1/2$ spin projections becomes the one with lowest energy. Therefore, the two channels with spin $1/2$ overscreen the effective impurity spin $1/2$. Signatures of NFL behaviour in both, the impurity contribution to the entropy and the equilibrium conductance, were previously reported¹⁶. In general, the behaviour of the model at low energies agrees with the corresponding one to the two-channel Kondo problem^{23,24}.

Finally, for negative values of the anisotropy D , which could be achieved by stretching the chain, there is no Kondo physics. This follows from the fact that the doublet $M_3 = \pm 3/2$ is now the fundamental one and the two channels with spin $1/2$ cannot flip the projections $\pm 3/2$ into each other. A residual entropy at zero temperature of $\ln(2)$ was found¹⁶ in this case and agrees with the non screened doublet $M_3 = \pm 3/2$ at the impurity site.

III. NUMERICAL RESULTS

In this section we present an accurate solution of the local spectral function by using the numerical renormalization group (NRG) as well as the differential conductance at the Co site obtained within the non crossing approximation (NCA).

For the numerical calculations, the complete set of the parameters determining the model was extracted from first principle calculations and are reported in Ref. 16. Here we summarize the parameters obtained. The total resonant level width $\Gamma = 0.6$ eV, is determined from the width of the peak of the degenerate xz, yz states above the Fermi energy. From the average position of these peaks, we define the charge transfer energy to be $E_{32} =$

$E_3 - E_2 = -0.3$ eV and finally, we take the conduction $5d_{xz,yz}$ bands extending from $-W$ to W with $W = 5$.

A. Impurity spectral density near the quantum critical point (NRG)

The impurity spectral function at the impurity site per channel and spin is given by $\rho_{\alpha\sigma}(\omega) = -\frac{1}{\pi}G_{\alpha\sigma}^r(\omega)$ where $G_{\alpha\sigma}^r(\omega)$ is the Fourier transform of the retarded Green function also per channel and spin,

$$G_{\alpha\sigma}^r(t) = -i\theta(t)\langle\{\hat{d}_{\alpha\sigma}(t), \hat{d}_{\alpha\sigma}^\dagger(0)\}\rangle. \quad (5)$$

The equilibrium conductance through the Co atom as a function of temperature, $G(T)$, depends on the total spectral function,

$$\rho(\omega) = \sum_{\alpha\sigma} \rho_{\alpha\sigma}(\omega), \quad (6)$$

and it is given by

$$G(T) = G_0 \frac{\pi\Delta A}{2} \int d\omega (-f'(\omega)) \rho(\omega), \quad (7)$$

where $G_0 = 2e^2/h$ is the quantum of conductance, $f(\omega)$ is the Fermi function, $\Delta = \frac{\Gamma}{2} = \Delta_L + \Delta_R$ represents the total resonant level width, and $A = 4\Delta_L\Delta_R/\Delta^2$ stands for the asymmetric connection between the Co atom and the left and right leads.

As it was previously mentioned, the model presents rich physics depending on the value of the anisotropy D . For positive D and low temperatures, the conductance was successfully scaled by $G(T) = a - b\sqrt{T}$, a behaviour similar to the two-channel Kondo model. Furthermore, $a = G(0)$, was found to be near G_0 , neglecting the small asymmetry between the leads given by the factor $A = 0.977$, see Fig. 4 of Ref. 16. This is half the value expected for a Fermi liquid with two channels in the unitary limit (Kondo regime). Consequently, within the overscreened regime, this seems to force the spectral density at the Fermi level (chosen to be at $\omega = 0$), to be $\rho(0) \sim \frac{2}{\pi\Delta}$ while the spectral weight per channel and spin seems to be $\rho_{\alpha\sigma}(0) \sim \frac{1}{2\pi\Delta}$. This agrees with the known rule for the 2CA impurity model²⁵, which can be obtained from our model in the limit $D \rightarrow +\infty$ and also for the 2CK model¹⁴. Several features in the Kondo resonance distinguish the 1CA from the 2CA spin-1/2 model⁴. Among others, i) the spectral weight for 2CA at $\omega = 0$ in the Kondo regime, is reduced to nearly half the value of 1CA $\rho_\sigma(0) \sim \frac{1}{\pi\Delta}$, ii) the resonance in 2CA is pinned at the Fermi level in contrast to the slight shift to positive energies found in the 1CA.

Within the underscreened regime, $D = 0$, the conductance at temperature $T = 0$ seems to approach to $2G_0$ which implies that the total spectral weight at the Fermi

level should be near $\rho(0) \sim \frac{4}{\pi\Delta}$. According to that, the spectral density at $\omega = 0$ per channel and spin surprisingly agrees with the specified by the generalized Friedel sum rule,²⁶ for two orbitals assuming an impurity occupation near 1 for each of them: $\rho_{\alpha\sigma}(0) \sim \frac{1}{\pi\Delta}$. This result differs from that of the well studied 1C underscreened Kondo effect in spin-1 molecules^{27,28}, where it was found that the phase shift has an additional term $\pi/2$ to that due to the contribution of the displaced electrons²⁷.

For $D < 0$, the projections $M_3 = \pm 3/2$ are not connected by the hopping processes with both channels. One has not a spin Kondo effect and there is no rule for the spectral density at the Fermi level. It is expected a continuous reduction of that weight when increasing $|D|$ as a consequence of the vanishing Kondo resonance. In the limit of $D \rightarrow -\infty$ the model splits into two different resonant models and Fermi liquid results could be used.

Important questions arise at this point: How does the spectral density evolve near to the transition point from negative to positive values of the anisotropy D ? Does the transition constitute a crossover or a quantum critical phase transition? Are there more energy scales involved in the transition in addition to the well known Kondo scale?

In what follows, we present the results of the spectral density from NRG calculations for different values of the anisotropy D . The results are obtained from full density matrix (fdm-) NRG calculations which exploited the SU(2) channel symmetry together with the abelian U(1) symmetries for total spin and total charge.²⁹⁻³¹ Further NRG specific parameters are $\Lambda = 4$ for the logarithmic discretization of the conduction bands together with z -averaging using $N_z = 2$,³² and a truncation energy $E_{tr} = 10$ in rescaled units (as defined in [31]). This resulted in retaining up to 16 000 multiplets (53 000 states) per iteration with exact diagonalization of state spaces of dimension up to 234 000 multiplets (846 000 states). The estimated resulting discarded weight of $\delta\rho < 10^{-15}$ indicates numerically well-converged data.³³

We start by defining the Kondo temperature, T_K , for $D = 0$ as the half width at the half maximum of the spectral density. For the model parameters representing the trimer it was found to be $T_K \approx 7 \cdot 10^{-6}$ eV.

In Fig. 2 we show the impurity spectral density per channel and spin for several positive values of the anisotropy D in units of T_K . By analogy with the Anderson model, the spectral data is scaled by $\pi\Delta$. In addition to the peak at the charge transfer energy at $\omega = E_{32}$, the spectral density exhibits two shoulders or satellite peaks at energies related with the anisotropy at $\omega = \pm D$ for $D > T_K$. These energies are indicated with arrows in the lower panel, corresponding to negative frequencies. Within the underscreened regime, as it was previously mentioned, the maximum of the spectral density at low energy roughly agrees with the expected one for FL behaviour. From the Friedel sum rule, one would expect $\pi\Delta\rho_{\alpha\sigma}(0) = \sin^2(\pi\langle n_{\alpha\sigma} \rangle)$ ²⁶ that is near to the result reported in Fig. 2 for an occupation of the Co atom per

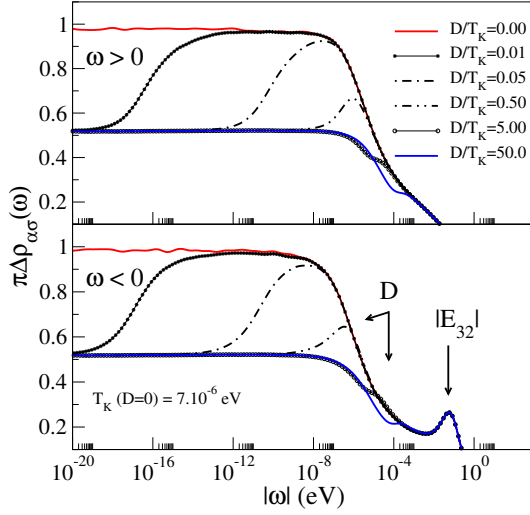


FIG. 2: (color online). Spectral density of the Co atom as a function of frequency in a logarithmic scale for different values of D (NRG). The upper and lower panels show the data for positive and negative ω respectively. The arrows stand for the charge transfer energy E_{32} and the anisotropy D .

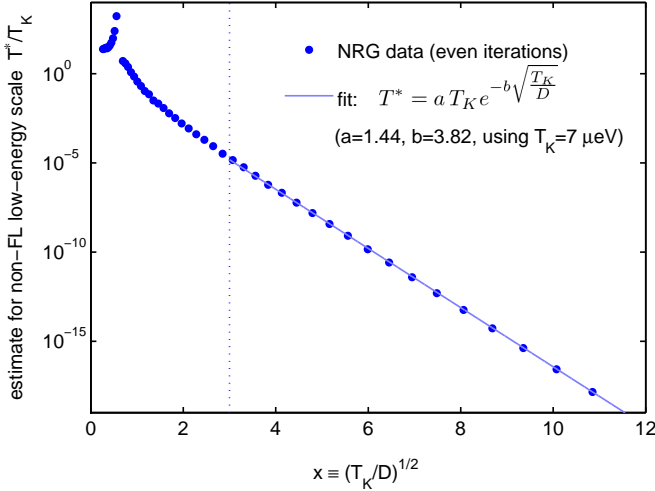


FIG. 3: (color online). Analysis of the low-energy scale T^* extracted from the NRG data (using even iterations n , with similar data and conclusions for odd iterations [not shown]). For the determination of T^* , the exponential convergence of the rescaled and iteratively subtracted ground state energy $E_0^{(n)}$ at iteration n deep into the low-energy fixed point was extrapolated towards larger energies (smaller n), such that $\Delta \tilde{E}_0^{(n^*)} := 1$ (in rescaled energies) with $\Delta \tilde{E}_0^{(n)}$ the plain exponential fit to $|E_0^{(n)} - E_0^{(\infty)}| < 0.01$. With this, the low energy scale $T^* := \Lambda^{-n^*/2}$ was determined individually for each value of the anisotropy D . Finally, the fit to the analytical expression for T^* was carried out for $x > 3$ (indicated by the vertical dotted line), i.e. $D < 0.11 T_K$.

channel and spin $\langle n_{\alpha\sigma} \rangle \simeq 1/2$. Using the real parameters representing the system shown in Fig. 1b, we obtain $\langle n_{\alpha\sigma} \rangle = 0.428$. Therefore, some degree of intermediate valence is present which would lead to a 5% lower value, i.e. $\pi \Delta \rho_{\alpha\sigma}(0) \simeq 0.95$. To the best of our knowledge, however, there are no exact results for the spectral weight at $\omega = 0$ for this kind of model, because it is expected to be a singular FL, in which the Friedel sum rule is not valid. In the case of the 1C underscreened spin $S = 1$, D. Logan *et al.* have found, on the basis of NRG calculations, that when the total impurity occupation, $\langle n_{imp} \rangle$, tends to 2, the normalized spectral weight at the Fermi level, $\pi \Delta \rho_{\alpha\sigma}(0)$, approaches 1 instead of zero as expected for a FL²⁷.

When the anisotropy D goes from $D = 0$ to $D > 0$, the spectral weight at the Fermi level is reduced suddenly to half its value. As it was previously mentioned, this agrees with the results expected for the 2CA model. When D turns positive, there is a new low-energy scale entering the system which controls the crossover from the underscreened to overscreened phases. An analysis of the low-energy spectrum as shown in Fig. 3, clearly suggests for $D \ll T_K$ the asymptotic form

$$T^* = a T_K e^{-b(T_K/D)^{1/2}}, \quad (8)$$

with a and b some dimensionless constants of order 1. It is interesting to note that in the case of 1C underscreened spin-1 model including anisotropy, a similar scale was found²⁸.

As it can be seen in Fig. 4, for $D \gg T_K$, the spectral weight continuously increases when the energy approaches to zero. However, for $D < T_K$ the spectral weight increases until $|\omega| \sim T^*$. For $|\omega| < T^*$ a dip is opened and the spectral density $\rho_{\alpha\sigma}(0)$ is suppressed to nearly half its value for $D = 0$. In Fig. 4 we show this peculiar behaviour for two selected values of the ratio, $D/T_K = 0.5$ and $D/T_K = 0.05$.

The results presented in Fig. 2 and Fig. 4 demonstrate that a QCP separating the overscreened and underscreened phases is present and NFL properties are obtained for any $D > 0$.

Finally, in Fig. 5 we present the results for negative values of the anisotropy D . As it can be seen, the spectral weight at the Fermi energy is continuously reduced when the values of $|D|$ are increased. This is expected due to the vanishing Kondo effect and follows from the fact that there is no spin-flip processes connecting the $M_3 = \pm 3/2$ projections.

B. Non equilibrium transport properties (NCA)

In this section we analyse the differential conductance, $G(T, V)$, through the Co atom when a finite bias voltage is applied to the system. For this purpose we calculated the current through the Co atom for each temperature as a function of bias voltage, $I(V)$, being $G = dI/dV$.

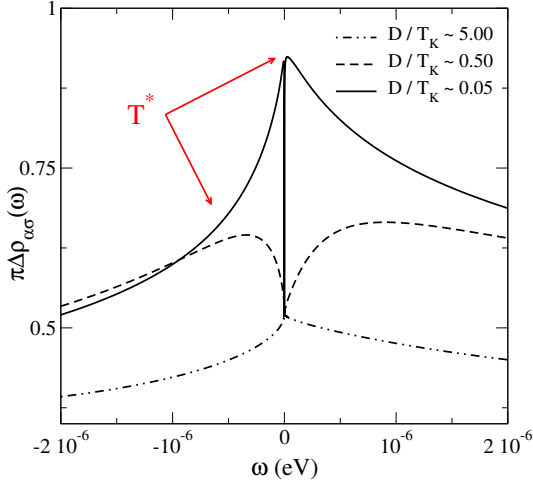


FIG. 4: (color online). Spectral density per channel and spin for different values of the ratio D/T_K (NRG).

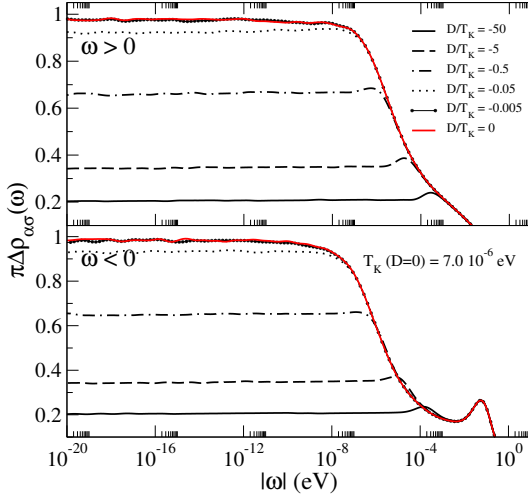


FIG. 5: (color online). Spectral density per channel and spin for different negative values of the ratio D/T_K (NRG).

The current per channel can be expressed in terms of the corresponding spectral density³⁴ obtained in the presence of the two different chemical potentials μ_L and μ_R ,

$$I_\alpha(V) = \frac{2\pi e}{h} \frac{\Gamma_L \Gamma_R}{\Gamma_L + \Gamma_R} \sum_\sigma \int d\omega [f_L(\omega) - f_R(\omega)] \rho_{\alpha\sigma}(\omega). \quad (9)$$

While for the equilibrium situation we obtain the spectral density exactly by using the NRG, within the non equilibrium one we employ the non crossing approximation, NCA, to solve the model. To apply the NCA we introduce auxiliary bosons for the triplets ($t_{\alpha M_2}$) and auxiliary fermions (q_{M_3}) for the quadruplet. In terms of the auxiliary operators the Hamiltonian in Eq.(1) takes the form

$$H_{\text{eff}} = (E_3 + \frac{D}{2} M_3^2) \sum_{M_3} q_{M_3}^\dagger q_{M_3} + E_2 \sum_{\alpha M_2} t_{\alpha M_2}^\dagger t_{\alpha M_2} + \sum_{\nu k \alpha \sigma} \epsilon_{\nu k} c_{\nu k \alpha \sigma}^\dagger c_{\nu k \alpha \sigma} + \sum_{\alpha \nu k \sigma} V_\nu \langle \frac{3}{2} M_3 | \frac{1}{2}; M_2 \sigma \rangle (q_{M_3}^\dagger t_{\alpha M_2} c_{\nu k \alpha \sigma} + \text{H.c.}). \quad (10)$$

The expression for the physical operators $d_{\alpha\sigma}^\dagger$ in terms of auxiliary particles are given by

$$d_{\alpha\uparrow}^\dagger = q_{3/2}^\dagger t_{\bar{\alpha},+1} + \sqrt{\frac{2}{3}} q_{1/2}^\dagger t_{\bar{\alpha},0} + \sqrt{\frac{1}{3}} q_{-1/2}^\dagger t_{\bar{\alpha},-1}, \quad (11)$$

$$d_{\alpha\downarrow}^\dagger = q_{-3/2}^\dagger t_{\bar{\alpha},-1} + \sqrt{\frac{2}{3}} q_{-1/2}^\dagger t_{\bar{\alpha},0} + \sqrt{\frac{1}{3}} q_{1/2}^\dagger t_{\bar{\alpha},+1} \quad (12)$$

Since only one state should be occupied at each time, the total operator number of auxiliary particles must satisfy the following constraint

$$\sum_{M_3} q_{M_3}^\dagger q_{M_3} + \sum_{\alpha M_2} t_{\alpha M_2}^\dagger t_{\alpha M_2} = 1. \quad (13)$$

The spectral density associated with the operator $d_{\alpha\sigma}^\dagger$ can be obtained by convolution of the greater and lesser Green functions of the auxiliary particles. For instance, the $\rho_{\alpha\uparrow}(\omega)$ is given by

$$\rho_{\alpha\uparrow}(\omega) = \frac{-1}{4\pi^2 Q} \int d\omega' \{ (G_{3/2}^>(\omega + \omega') G_{\alpha,+1}^<(\omega') - G_{3/2}^<(\omega + \omega') G_{\alpha,+1}^>(\omega')) + \frac{2}{3} (G_{1/2}^>(\omega + \omega') G_{\alpha,0}^<(\omega') - G_{1/2}^<(\omega + \omega') G_{\alpha,0}^>(\omega')) + \frac{1}{3} (G_{-1/2}^>(\omega + \omega') G_{\alpha,-1}^<(\omega') - G_{-1/2}^<(\omega + \omega') G_{\alpha,-1}^>(\omega')) \}, \quad (14)$$

being Q the impurity canonical partition function

$$Q = \frac{-i}{2\pi} \int d\omega (\sum_{M_3} G_{M_3}^<(\omega) - \sum_{\alpha, M_2} G_{\alpha, M_2}^<(\omega)). \quad (15)$$

A similar expression allows to obtain $\rho_{\alpha\downarrow}(\omega)$ and, in absence of an applied magnetic field, as it is actually our case, $\rho_{\alpha\downarrow}(\omega) = \rho_{\alpha\uparrow}(\omega)$.

In order to obtain the greater auxiliary Green function, a selfconsistent loop for the selfenergies have to be solved,

$$\begin{aligned}
\Sigma_{q_{3/2}}^>(\omega) &= \frac{1}{2\pi} \sum_{\nu\alpha} \Gamma_{\nu\alpha\uparrow} \int d\omega' f(\omega' - \omega + \nu_\mu) G_{\tilde{\alpha},+1}^>(\omega') \\
\Sigma_{q_{-3/2}}^>(\omega) &= \frac{1}{2\pi} \sum_{\nu\alpha} \Gamma_{\nu\alpha\downarrow} \int d\omega' f(\omega' - \omega + \nu_\mu) G_{\tilde{\alpha},-1}^>(\omega') \\
\Sigma_{q_{1/2}}^>(\omega) &= \frac{1}{6\pi} \sum_{\nu\alpha} \int d\omega' f(\omega' - \omega + \nu_\mu) [2\Gamma_{\nu\alpha\uparrow} G_{\tilde{\alpha},0}^>(\omega') \\
&\quad + \Gamma_{\nu\alpha\downarrow} G_{\tilde{\alpha},1}^>(\omega')] \\
\Sigma_{q_{-1/2}}^>(\omega) &= \frac{1}{6\pi} \sum_{\nu\alpha} \int d\omega' f(\omega' - \omega + \nu_\mu) [2\Gamma_{\nu\alpha\downarrow} G_{\tilde{\alpha},0}^>(\omega') \\
&\quad + \Gamma_{\nu\alpha\uparrow} G_{\tilde{\alpha},-1}^>(\omega')] \quad (16)
\end{aligned}$$

together with the non-equilibrium Dyson equations

$$G_i^>(\omega) = G_i^r(\omega) \Sigma_i^>(\omega) G_i^a(\omega), \quad (17)$$

where the retarded Green functions are given by

$$G_i^r(\omega) = \frac{1}{\omega - \epsilon_i - \Sigma_i^r(\omega)}. \quad (18)$$

Within the NCA, the retarded and greater selfenergies are related by

$$\Sigma_i^>(\omega) = 2i \operatorname{Im} \Sigma_i^r(\omega). \quad (19)$$

An independent loop for the lesser selfenergies is needed to get the partition function and the lesser Green functions. The loop is closed using again the equations Eq.(17),

$$\begin{aligned}
\Sigma_{q_{3/2}}^<(\omega) &= -\frac{1}{2\pi} \sum_{\nu\alpha} \Gamma_{\nu\alpha\uparrow} \int d\omega' f(\omega - \omega' - \nu_\mu) G_{\tilde{\alpha},+1}^<(\omega') \\
\Sigma_{q_{-3/2}}^<(\omega) &= -\frac{1}{2\pi} \sum_{\nu\alpha} \Gamma_{\nu\alpha\downarrow} \int d\omega' f(\omega - \omega' - \nu_\mu) G_{\tilde{\alpha},-1}^<(\omega') \\
\Sigma_{q_{1/2}}^<(\omega) &= -\frac{1}{6\pi} \sum_{\nu\alpha} \int d\omega' f(\omega - \omega' - \nu_\mu) [2\Gamma_{\nu\alpha\uparrow} G_{\tilde{\alpha},0}^<(\omega') \\
&\quad + \Gamma_{\nu\alpha\downarrow} G_{\tilde{\alpha},1}^<(\omega')] \\
\Sigma_{q_{-1/2}}^<(\omega) &= -\frac{1}{6\pi} \sum_{\nu\alpha} \int d\omega' f(\omega - \omega' - \nu_\mu) [2\Gamma_{\nu\alpha\downarrow} G_{\tilde{\alpha},0}^<(\omega') \\
&\quad + \Gamma_{\nu\alpha\uparrow} G_{\tilde{\alpha},-1}^<(\omega')] \quad (20)
\end{aligned}$$

The equilibrium properties can be simply obtained by setting $\mu_L = \mu_R = 0$ when solving the selfconsistent loop for the lesser and greater selfenergies.

In the numerical procedure to solve the previous NCA equations, we follow the computational algorithms, that ensure an accurate solution of the problem, detailed in Refs. 35–37.

In what follows we present the NCA results for the impurity entropy, spectral density and differential conductance for different values of the anisotropy D .

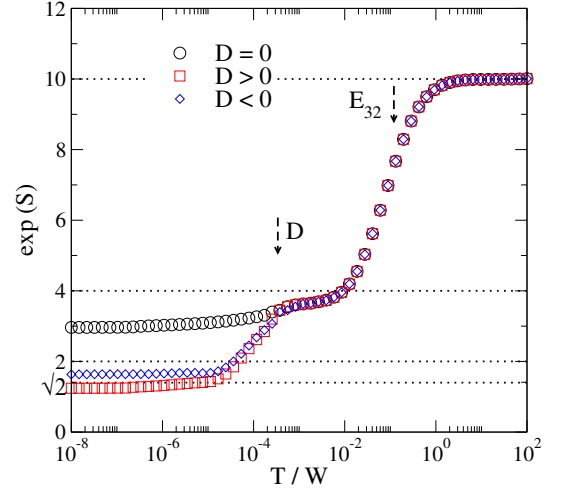


FIG. 6: (color online). NCA impurity contribution to the entropy (at equilibrium) as a function of temperature for $D = 0$ and $D = \pm 0.0017\text{eV}$. Energies are given in units of the half bandwidth W .

In Fig. 6 we show the Co contribution to the entropy as a function of temperature for different values of the anisotropy D . The latter is calculated through numerical differentiation of the free energy³⁶. At high temperatures all the impurity degrees of freedom are active due to the charge fluctuations and therefore the entropy tends to $S = \ln(10)$ (in units of the Boltzmann constant k_B). As the temperature is lowered, the charge transfer is frozen and the only active degrees of freedom correspond to the local moment regime characterized by a local spin 3/2, and therefore a plateau appears with $S \approx \ln(4)$. When the temperature reaches $T \sim |D|$, the three different regimes are separated. At low enough temperatures, our model is expected to have entropy $S = \ln(2)$ when $D < 0$ reflecting the presence of two decoupled local moments. The same low temperature limit should be reached for the underscreened, $D = 0$, regime in which a doublet is still present (see Fig. 3 of Ref. 16). As it can be seen from Fig. 6, the NCA overestimates the expected value for the underscreened case. This is related to the neglected vertex correction within this approach. Surprisingly, the NCA entropy at low temperatures for negative D is closer to the expected one. Within the overscreened regime, the NCA entropy at low temperatures gives the correct residual value of $S \sim \frac{1}{2} \ln(2)$. It is well known that NCA is a reliable technique for the overscreened 2CA model. Regarding the thermodynamic properties, the residual entropy and the scaling behaviour of the static magnetic susceptibility, among others, have been successfully compared with exacts Bethe ansatz results⁵.

In Fig. 7 we show the NCA results for the spectral density at equilibrium conditions for the same set of parameters as in Fig. 2 for several values of D . For simplicity, we show only the negative frequency data. When comparing the NCA results with the NRG correspond-

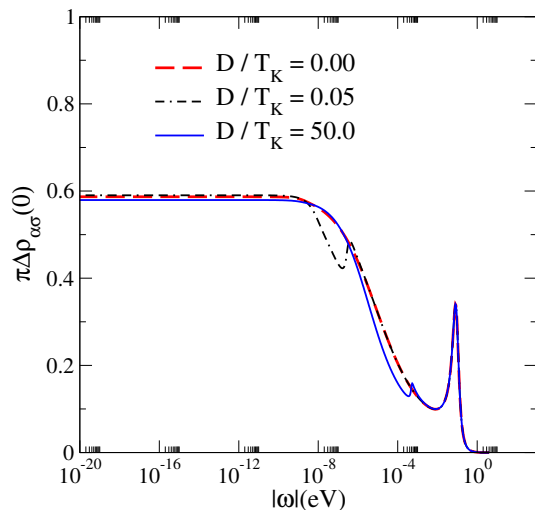


FIG. 7: (color online). NCA spectral density per channel and spin for different values of the ratio D/T_K at equilibrium.

ing ones, it is clear that for $D = 0$, the NCA spectral weight at the Fermi level is strongly underestimated. This can be understood as follows. Within the underscreened regime, $D = 0$, a scaling in the hybridization $\Delta' = \Delta/3$ in the system of NCA selfconsistent equations Eq.(16), Eq.(20) and Eq.(15) leads to an identical system in which the ground and excited states have degeneracies $N = 4$ and $M = 6$, respectively. For such a model, the NCA spectral density at the Fermi level is expected to be $\rho(0) \sim \frac{2\pi}{(N+M)^2\Delta'}$, (see appendix B of Ref. 5),⁴⁰. We have verified that our calculations satisfy this rule. In addition, when D becomes positive but lower than the Kondo temperature associated with the underscreened case, the low-energy scale T^* is completely absent. On the other hand, for large enough negative values of the anisotropy (not shown) no Kondo resonance is expected. However the NCA spectral function develop a spurious spike at the Fermi level at low temperatures, in analogy with other cases of systems with a non degenerate ground state in absence of hybridization (see Fig. 3 of Ref. 37). Therefore, we conclude from the comparison with NRG that the NCA approach does not represent a suitable technique for a quantitative and even qualitative treatment of the problem when $D < T_K$.

Regarding the spectral function for $D \geq T_K$, we found the expected asymptotic low energy dependence $\sim \sqrt{\omega}$ in the limit $\omega \rightarrow 0$ and a slight overestimation of the spectral weight at the Fermi level at very low temperatures. On the other hand, for dynamical properties the NCA reproduces the exact power law at low energies of all 4-point auxiliary correlation functions, like is the case of the spectral density^{4,36}. Specifically, for transport properties like equilibrium conductance and differential conductance, both depending on the spectral density, the NCA gives the exact non trivial \sqrt{T} and \sqrt{V} dependence respectively^{38,39}.

In Fig. 8 we present the total differential conductance

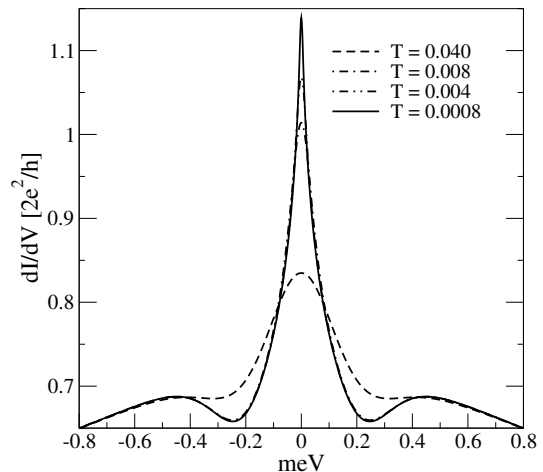


FIG. 8: Total differential conductance as a function of the bias voltage for several values of temperature. The model parameters correspond to the real configuration of the trimer sketched in Fig.1(b) with the parameters given in the text. Temperatures are given in units of meV.

through the Co atom for the real parameters in the trimer geometry as a function of the bias voltage V and for several temperatures. While for $T = V = 0$, a value of $2G_0$ is expected in the general case of two independent conductance channels, we obtain nearly half of it in agreement with NRG. This is, once again, an additional verification of the non trivial 2C behaviour. The zero-bias anomaly (ZBA) reflects the low-lying energy dependence of the spectral function and a \sqrt{V} behavior is explicitly shown in the next two figures. A slight overestimation of the unitary limit is also obtained and follows from the corresponding one of the spectral weight at the Fermi level. In addition to the ZBA, the differential conductance exhibits two broad peaks located at $eV \sim \pm 2D$, related with the excited states $\pm 3/2$.

Affleck and Ludwig's conformal field theory (CFT) solution of the 2CK problem suggested that a scaling of the differential conductance $G(T, V)$ as a function of T and V should be possible with the form

$$G(T, V) - G(T, 0) = BT^{1/2}H\left(A\frac{eV}{k_B T}\right), \quad (21)$$

where H is an universal function with the conditions $H(0) = 0$ and $H(x) \sim x^{1/2}$ for $x \gg 1$, and A, B are non-universal constants (i.e. sample-dependent). The constant B is determined from the equilibrium conductance⁴².

Figure 9 shows the scaling plot of $G(T, V)$ as a function of $(eV/k_B T)^{1/2}$ for a general set of parameters and for several values of the anisotropy D . From the half width at the half maximum of the Kondo resonance of the spectral function at equilibrium we found $T_K^{D=0} \sim 0.00001$ in units of the bandwidth W . As it is clear from the figure, when the anisotropy D becomes $D \geq T_K^{D=0}$ the curves

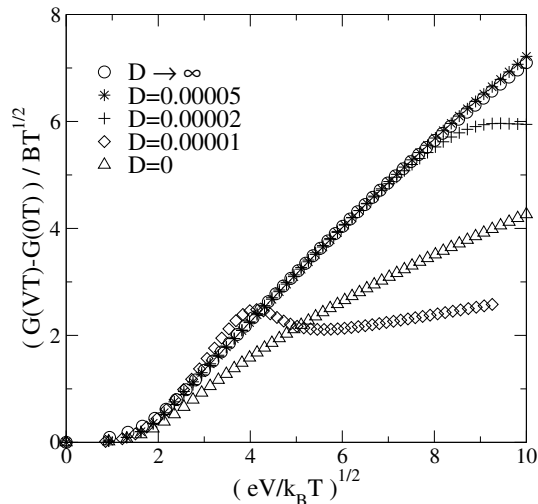


FIG. 9: Scaling plot of the differential conductance $G(T, V)$ for different values of the anisotropy D at a very low temperature, $T = 0.001T_K$. Parameters are $W = 1$, $E_{32} = -0.67$, $\Delta = 0.225$. Here, we define T_K from the half width at the half maximum of the Kondo resonance of the spectral function at equilibrium.

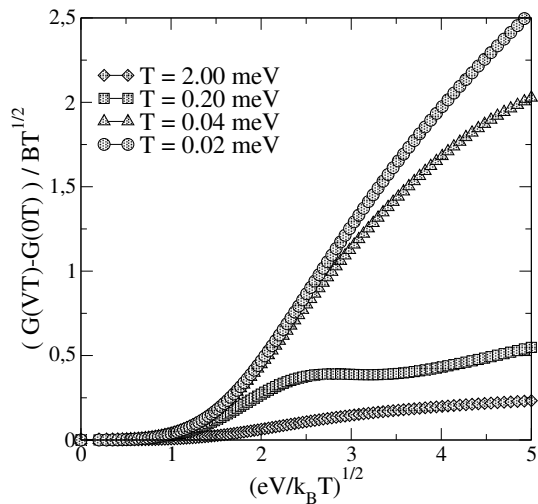


FIG. 10: Scaling plot of the differential conductance $G(T, V)$ for different temperatures for the real parameters corresponding to the trimer configuration.

collapse onto a single curve proportional to $(eV/k_B T)^{1/2}$. For $D \geq T_K^{D=0}$ the differential conductance follows the CFT scaling function expected for the 2CK model.

In Fig. 10 we show the differential conductance as a function of $(eV/k_B T)^{1/2}$ for the real parameters corresponding to the trimer configuration and for several temperatures. When the charge fluctuations are inhibited due to the decreasing temperature, the $G(T, V)$ through the Co atom displays the 2C scaling behaviour.

IV. CONCLUSIONS

In summary, extending a previous study of the entropy and equilibrium conductance through a Co atom coupled to monoatomic Au chains with a four-fold symmetric leads, we have presented a comprehensive study of the equilibrium spectral density using NRG and the non-equilibrium conductance in the non-Fermi liquid regime using NCA.

We found that a quantum critical point at the anisotropy value $D = 0$ takes place. The three different phases, underscreened, overscreened and no Kondo phases are characterized by the weight of the Kondo resonance at the Fermi level. Within the underscreened Kondo regime, the value of the spectral density per channel and spin is given approximately by $\rho_{\alpha\sigma}(0) \sim \frac{1}{\pi\Delta}$ in analogy to the ordinary Kondo model, although the system is expected to be a singular Fermi liquid. On the other hand, within the overscreened regime, the spectral weight is reduced to half this value, $\rho_{\alpha\sigma}(0) \sim \frac{1}{2\pi\Delta}$. We also found that the Kondo temperature of the underscreened phase, T_K plays an important role in the cases of positive values of D . When $0 < D \leq T_K$ the way in which the system enters into the 2C fixed point is mediated by a new energy scale T^* , that depends exponentially on the ratio T_K/D .

We also present a solution of the model by means of the non-crossing approximation not only at equilibrium but also for non-equilibrium situations such as transport properties as a function of the bias voltage. Our results suggest that the only phase in which the NCA becomes a reliable method is the overscreened regime in which the anisotropy value should be $D \geq T_K$. In particular, the NCA for $D = 0$ underestimates the spectral weight at the Fermi level in a 40% and for the cases in which $0 < D \leq T_K$ the low-energy scale T^* is missed. In contrast, for $D \geq T_K$, corresponding to the regime of parameters for which 2C physics is more evident, we have verified that the NCA gives the correct residual entropy and (except for a slight overestimation), it also gives the correct value of the spectral densities at the Fermi level. This suggests that the NCA is a reliable approximation to study the overscreened regime also at finite bias voltage, for which our NRG methods are not appropriate.

For small values of temperature T and bias voltage V , the obtained differential conductance agrees with the predictions of conformal-field theory for the 2CK model. Specifically, we show that for realistic parameters corresponding to the system of Fig. 1(b) the conductance through the Co atom as a function of the bias voltage follows a \sqrt{V} dependence, in agreement with the behavior expected for this kind of non Fermi liquid models. Furthermore a universal scaling behaviour as a function of $(eV/k_B T)^{1/2}$ is obtained.

Our results confirm the rich physics of the model. We expect that our study can stimulate experimental studies on similar systems.

V. ACKNOWLEDGMENTS

This work was partially supported by PIP No 112-200801-01821, 00273 and 00258 of CONICET, and PICT 2010-1060 of the ANPCyT, Argentina. AW acknowledges support from the German Research Foundation (TR-12,

SFB631, NIM, and WE4819/1-1).

References

- ¹ J. Kondo, *Prog. Theor. Phys.* **32** 37 (1964).
- ² P. W. Anderson, *Phys. Rev.* **124**, 41 (1961).
- ³ D. Goldhaber-Gordon et al., *Nature* (London), **391**, 156 (1998); D. Goldhaber-Gordon et al., *Phys. Rev. Lett.* **81**, 5225 (1998).
- ⁴ D. L. Cox and A. Zawadowski, *Adv. in Phys.* **47** 599 (1998).
- ⁵ Tae-Suk Kim and D. L. Cox, *Phys. Rev. B* **55** 12594 (1997).
- ⁶ Ph. Nozières and et A. Blandin, *J. Phys. France* **41**, 193 (1980).
- ⁷ H. J. Schulz, Proceedings of Les Houches Summer School LXI", ed. E. Akkermans, G. Montambaux, J. Pichard, et J. Zinn-Justin (Elsevier, Amsterdam, 1995), p.533. arXiv:cond-mat/9503150
- ⁸ Y. Oreg and D. Goldhaber-Gordon, *Phys. Rev. Lett.* **90**, 136602 (2003).
- ⁹ R. M. Potok, I. G. Rau, H. Shtrikman, Y. Oreg, and D. Goldhaber-Gordon, *Nature* **446**, 167 (2007).
- ¹⁰ M. Pustilnik, L. Borda, L. I. Glazman and J. von Delft, *Phys. Rev. B* **69**, 115316 (2004)
- ¹¹ S. Florens and A. Rosch, *Phys. Rev. Lett.* **92**, 216601 (2004).
- ¹² N. Andrei and C. Destri, *Phys. Rev. Lett.* **52**, 364 (1984); A. M. Tvelick and P. B. Wiegmann, *Z. Phys. B* **54**, 201 (1984).
- ¹³ G. Zaránd, C-H. Chung, P. Simon, and M. Vojta, *Phys. Rev. Lett.* **97**, 166802 (2006)
- ¹⁴ A. K. Mitchell, E. Sela, and D. E. Logan, *Phys. Rev. Lett.* **108**, 086405 (2012).
- ¹⁵ A. M. Tsvelik and Wei-Guo Yin, *Phys. Rev. B* **88**, 144401 (2013).
- ¹⁶ S. Di Napoli, A. Weichselbaum, P. Roura-Bas, A. A. Aligia, Y. Mokrousov, and S. Blügel, *Phys. Rev. Lett.* **110** 196402 (2013).
- ¹⁷ K. G. Wilson, *Rev. Mod. Phys.* **47**, 773 (1975). R. Bulla, T. Costi, and T. Pruschke, *Rev. Mod. Phys.* **80**, 395 (2008).
- ¹⁸ Di Napoli, S., Barral, M. A., Roura-Bas, P., Aligia, A. A., Mokrousov, Y. and Llois, A. M. *IEEE transactions on magnetics* **49**(8), 4683 (2013).
- ¹⁹ W. H. A. Thijssen, D. Marjenburgh, R. H. Bremmer, and J. M. van Ruitenbeek, *Phys. Rev. Lett.* **96** 026806 (2006).
- ²⁰ A. A. Aligia and T. Kroll, *Phys. Rev. B* **81**, 195113 (2010).
- ²¹ A. A. Aligia, C. A. Balseiro and C. R. Proetto, *Phys. Rev. B* **33**, 6476 (1986)
- ²² P. Mehta, N. Andrei, P. Coleman, L. Borda, and G. Zaránd, *Phys. Rev. B* **72**, 014430 (2005).
- ²³ I. Affleck, A. W. W. Ludwig, H.-B. Pang, and D. L. Cox, *Phys. Rev. B* **45**, 7918 (1992).
- ²⁴ V. J. Emery and S. Kivelson, *Phys. Rev. B* **46**, 10812 (1992).
- ²⁵ F. B. Anders, *Phys. Rev. B* **71**, 121101(R) (2005).
- ²⁶ A. Yoshimori and A. Zawadowski, *J. Phys. C* **15**, 5241 (1982).
- ²⁷ D. E. Logan, C. J. Wright and M. R. Galpin, *Phys. Rev. B* **80** 125117 (2009).
- ²⁸ P. S. Cornaglia, P. Roura Bas, A. A. Aligia and C. A. Balseiro, *Europhys. Lett.* **93** 47005 (2011).
- ²⁹ A. Weichselbaum and J. von Delft, *Phys. Rev. Lett.* **99** 076402 (2007).
- ³⁰ A. Weichselbaum, *Ann. Phys. (Amsterdam)* **327**, 2972 (2012).
- ³¹ A. Weichselbaum, *Phys. Rev. B* **86** 245124 (2012).
- ³² M. Yoshida, M. A. Whitaker, and L. N. Oliveira, *Phys. Rev. B* **41**, 9403 (1990). R. R. Zitko and T. Pruschke, *Phys. Rev. B* **79**, 085106 (2009).
- ³³ A. Weichselbaum, *Phys. Rev. B* **84** 125130 (2011).
- ³⁴ Meir Y and Wingreen N S 1992 *Phys. Rev. Lett.* **68** 2512.
- ³⁵ Wingreen N S and Meir Y, *Phys. Rev. B* **49** 11040 (1993).
- ³⁶ M. H. Hettler, J. Kroha and S. Hershfield, *Phys. Rev. B* **58** 5649 (1998).
- ³⁷ P. Roura Bas and A. A. Aligia, *J. Phys.: Condens. Matter* **22** (2010).
- ³⁸ Matthias H. Hettler, Johann Kroha, and Selman Hershfield, *Phys. Rev. Lett.* **73** 1967 (1994).
- ³⁹ P. Roura-Bas, S. Di Napoli and A. A. Aligia, *Journal of Physics: Conference Series* **480** (2014) 012013.
- ⁴⁰ An additional factor 2 was included due to the definition of the physical operator in Eq.(11).
- ⁴¹ A. W. W. Ludwig, *Int. Jour. Mod. Phys. B* **8** (1994), 347 and references therein.
- ⁴² See Eq. (27) of Ref. ³⁶.